PERGAMON

International Journal of Heat and Mass Transfer 44 (2001) 143–153

International Journal of HEAT and MASS TRANSFER

www.elsevier.com/locate/ijhmt

Interactions between laser-activated nucleation sites in pool boiling

Iztok Golobič*, Henrik Gjerkeš

Faculty of Mechanical Engineering, University of Ljubljana, Aškerčeva 6, 1000 Ljubljana, Slovenia

Received 3 September 1999; accepted 18 February 2000

Abstract

A technique of activating nucleation sites by heating them with laser beams has been developed to enable direct measurements of interactions between active nucleation sites. Interactions between two, three and four simultaneously active nucleation sites in various arrangements on 25 μm thick copper and titanium foil in saturated water pool boiling were studied experimentally. The experiments were performed with heated spot diameters ranging from 1.66 to 5.23 mm and heat fluxes up to 560 kW/m^2. The interaction between two laser activated nucleation sites occurs as a net decrease of activity of both sites. It is possible that the activity of both decreases simultaneously, or the activity of one increases, while the activity of the other nucleation site decreases simultaneously. Similar behaviour was also observed in the experiments involving three and four active nucleation sites. In the extreme case, one nucleation site can deactivate the other. Local surface characteristics can play an important role in the interaction between the nucleation sites.

Keywords: Boiling; Experimental; Nucleonics

1. Introduction

Boiling, as the process of heat and mass transfer, has been intensively researched for at least two hundred years [1], and several empirical or phenomenological correlations have been developed. However, the process is extremely complex [2]. In recent years prevalent mechanistic approach [3,4] is based on the underlying fundamental physical processes, where the bubble boiling is treated as a local-instantaneous conjugated problem including spatio-temporal behaviour of the wall superheat in the vicinity of nucleation centres and its consequences for instantaneous heat flux. The understanding of behaviour of the nucleation site, as the basic boiling element and interactions between nucleation sites in connection with wall surface microstructure and topography, is therefore of key significance [5]. Their study requires the development of experimental methods for directly measuring local and spatial instantaneous characteristic on the boiling surface [6,7]. One such method is a developed technique of laser-heated thin metal foil, which enables the activation of one or more nucleation sites at an arbitrary location on a flat surface [8,9].

Chekanov [10] measured the interaction between two active nucleation sites at pool boiling of water, which he achieved with the aid of two heating rods in contact with the boiling surface. He determined that the activity of the nucleation sites in dependence on the sep-

* Corresponding author. Tel.: +386-61-1771-420; fax: +386-61-218-567.

E-mail address: iztok.golobic@uni-lj.si (I. Golobič).

0017-9310/01/$ - see front matter
PII: S0017-9310(00)00087-9

Nomenclature

$\mathscr{A}$	diffusive absorptivity
c	specific heat (J kg^{-1} K^{-1})
c_M, c_N	constants, Eqs. (11) and (12)
D_B	bubble departure diameter (m)
D_F	foil diameter (m)
D_H	heated spot diameter (m)
$D_{H,\infty}$	heated surrounding surface diameter (m)
f	bubble frequency (s^{-1})
f_0	bubble frequency of an isolated nucleation site (s^{-1})
h_{fg}	latent heat of vaporisation (J kg^{-1})
i_x, i_y, j_x, j_y	Cartesian co-ordinates of nucleation sites i and j (m)
$K_{LC,i}$	correction parameter for nucleation site i
M	non-dimensional distance from foil centre
m_x, m_y	Cartesian co-ordinates of the centre of heated surrounding surface (m)
N	non-dimensional distance from the centre of heated surrounding surface
P	laser beam power (W)
$\dot{Q}_L$	latent heat flow rate (W)
$\dot{Q}_{L,0}$	latent heat flow rate of an isolated nucleation site (W)
$\dot{Q}_{L,C}$	corrected latent heat flow rate (W)
q_H	heat flux in heated spot (W m^{-2})
$q_{H,\infty}$	heat flux in heated surrounding surface (W m^{-2})
r_A	arithmetic mean roughness (μm)
S	distance between two active nucleation sites (m)

Greek symbols

δ	foil thickness (m)
λ	thermal conductivity (W m^{-1} K^{-1})
ρ	density (kg m^{-3})
ρ_v	vapour density (kg m^{-3})
$(\rho c\lambda)^{0.5}$	effusivity (W s$^{0.5}$ m^{-2} K^{-1})

arating distance follows the gamma distribution and that, at reducing the distance between them, the nucleation sites first promote and then, at the smaller distances between them, inhibit each other. On the basis of CHF analysis on a small, laser-heated surface [9], we can estimate that in Chekanov's experiment, where heat flux was 2 and 5 MW/m^2, film boiling occurred, which may influence the results. Although many studies of interactions were conducted [5,11–13], and the densities of active nucleation sites at the surface were determined [14–17], the physical principle of the behaviour of the nucleation sites still has not been clearly explained.

The present paper describes the experimental observation of interactions between the artificially activated nucleation sites, obtained with laser heating a thin metal foil at saturated water pool boiling.

2. Experimental set up

Fig. 1(a) and (b) shows the experimental set-up. The vessel contained saturated boiling water at atmospheric pressure. A test section with metal foil was placed at the bottom of the vessel. It was in contact with the water on one side, while the other side was irradiated by laser beams.

A continuous wave Nd:YAG laser with a wavelength of 1064 nm and a maximum power of 70 W was used. The laser beam travelled through an opto-mechanical system, where it was adjusted to the desired characteristics. After exiting the laser, a non-polarised laser beam passed through a plano-convex lens (I) and fell onto a polarising beam splitter cube (III), where it split up into two differently polarised beams (A and B) of approximately equal power at an angle of 90°. Polarisation was necessary due to the use of variable attenuators (IV) which were used to set the power of beam (A) and beam (B) separately. After leaving the attenuators, the path of the two beams leading to the test section was determined by position of the mirrors (V) and (VIII). Mirrors (VIII) redirected the beams onto the metal foil, i.e., to the lower, dry part of the test section. The angles of the mirrors could be varied accurately around two axes using micrometer screws on the mirror mounts. By manually adjusting the angle of the mirrors (VIII) the angle of reflection of the laser beam was changed. In this manner it was possible to direct each beam to any spot on the lower part of the test section. A more detailed description of the technique of activating nucleation sites by laser heating in pool boiling can be found in Ref. [9].

At the configuration shown in Fig. 1(a), a lens (VI) was placed on the path of beam (A) and a laser beam splitter (VII) between mirrors (V) and (VIII). Translatory movement of lenses (I) and (VI) enabled the setting of diameters of beams (A) and (B) separately. Using a beam splitter, beam (A) was

split into beam (A1) and beam (A2), having equal power and equal diameter. Laser beams (A1) and (A2) were used to heat a surface with a diameter D_H ranging from 1.66 to 5.3 mm and with a heat flux q_H, while laser beam (B) heated the surrounding surface with a diameter $D_{H,\infty}$ ranging from 16 to 20 mm and with a heat flux $q_{H,\infty}$. Possible arrangement of heated spots in this configuration is shown in the inset of Fig. 1(a). If $q_{H,\infty} > 0$, the heat flux on the heated spot with a diameter D_H was the sum of both heat fluxes to this surface.

The opto-mechanical system shown in the configuration in Fig. 1(b) was used for experiments with three or four active nucleation sites without heating the surrounding surface. For this purpose lens (VI) was removed and a beam-expander (II) was added between lens (I) and the polarising beam splitter cube (III). A beam splitter (VII) and one mirror (VIII) were also added to the path of beam (B), in order to obtain another two equal beams (A3) and (A4). Laser beams (A1) to (A4) were used to heat four spots, arbitrarily located on the foil, with a diameter D_H ranging from 1.6 to 5.35 mm and with a heat flux q_H. Possible arrangement of four heated spots can be seen in the inset of Fig. 1(b). The opto-mechanical system is symmetrical in this configuration, so that all four heated spots have the same diameter D_H and the pairs of beams have equal power.

A photoelectric system was constructed to determine the diameter and position of the laser beams. Immediately below the test section where the laser beams hit, a silicon PIN photodiode with a very small active area, 0.56×0.56 mm, was installed on an XY translation stage with displacement accuracy of ± 4 μm. A photodiode changes the voltage of the output electrical current depending on its illumination. By changing the relative position of the photodiode with regard to the beam, the illumination of the photodiode changes. This is detected by measuring the output electrical voltage.

The experiments were conducted using a copper or a titanium foil with a thickness δ of 25 μm and a diameter D_F of 30 mm. Both foils had a commercial, standard surface finish. The surface roughness was measured according to ISO 4288 with a Hommel Tester T2000 and a TKL 100 sensor. Titanium foil roughness was $r_A = 0.10$ μm and the copper foil roughness was $r_A = 0.17$ μm. On dry side, where the laser beams hit, the foils were coated with a 10–12 μm thick layer of highly temperature-resistant mat black paint. Diffusive absorptivity of the mat black paint was measured with Labsphere RSA PE-19 integration

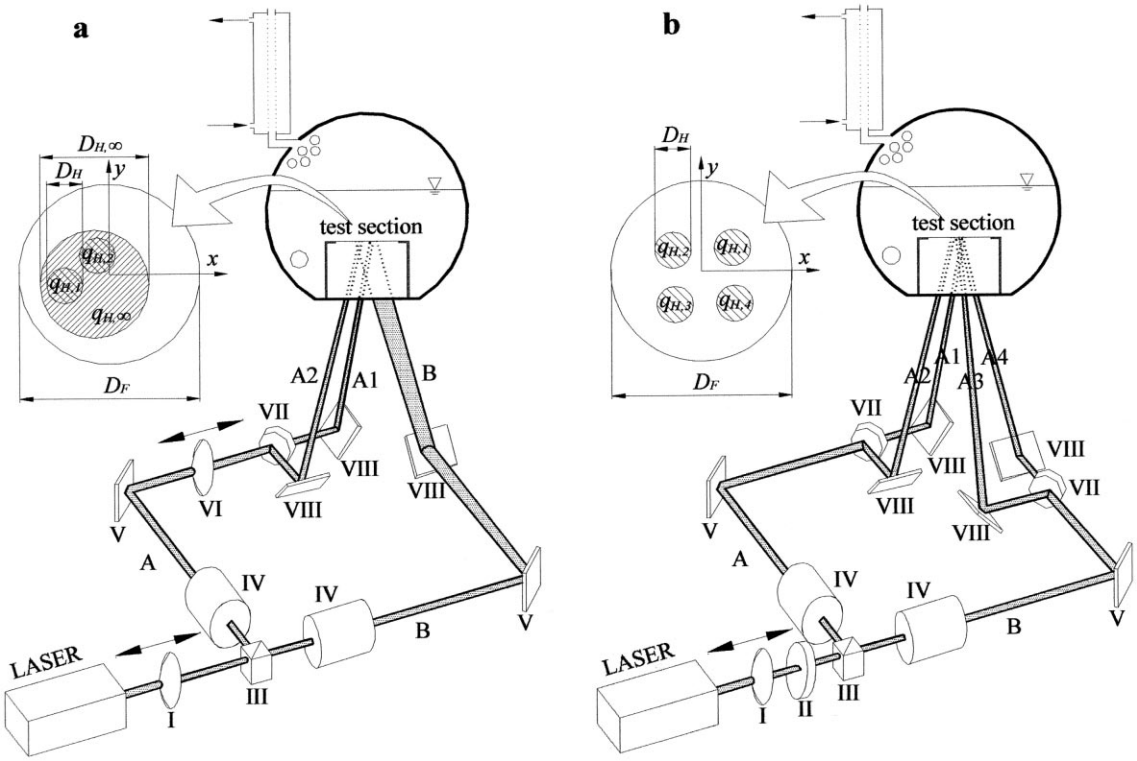

Fig. 1. Schematic diagram of used configurations of the experimental set up.

sphere and was determined to be $\mathscr{A} = 0.946$ at wavelength 1064 nm.

The heat fluxes $q_{H,i}$ and $q_{H,\infty}$ in the configurations shown in Fig. 1 were calculated using the following equations:

$$q_{H,i} = \frac{4}{\pi D_H^2}\mathscr{A} P_{Ai}, \tag{1}$$

$$q_{H,\infty} = \frac{4}{\pi D_{H,\infty}^2}\mathscr{A} P_B, \tag{2}$$

where P_{Ai} is the measured power of the laser beam (Ai) and P_B is the measured power of the laser beam (B) before they reach the test section. D_H is the measured diameter of the laser beam (Ai) and $D_{H,\infty}$ is the measured diameter of the laser beam (B).

Water was degassed by boiling in the test vessel for at least two hours prior to the beginning of the experiment. The temperatures of the fluid and the vapour above it were measured with NiCr–Ni thermocouples. All tests were performed at atmospheric pressure between 1.005 and 1.018 bar and at an average water temperature between 99 and 100°C.

The boiling experiments were recorded using a Sony Hi8 camcorder with a 48× zoom lens and a speed of 25 full frames per second. The recording was digitised and transferred to a computer on which it was possible to split full frames into even and odd frames, thus yielding a succession of images with a temporal resolution of 20 ms.

A diameter and frequency of bubbles and released latent heat flow rate of the nucleation site were determined by analysing the video sequences. The calculated measuring uncertainty in determining latent heat flow rate was within ±14.3% in the most unfavourable measurements.

The interaction between nucleation sites was observed using two heated spots at various distances between them, and three or four heated spots arranged in a line or in a quadrangle. An image of four active nucleation sites, activated with four heated spots, arranged in line, is shown in Fig. 2.

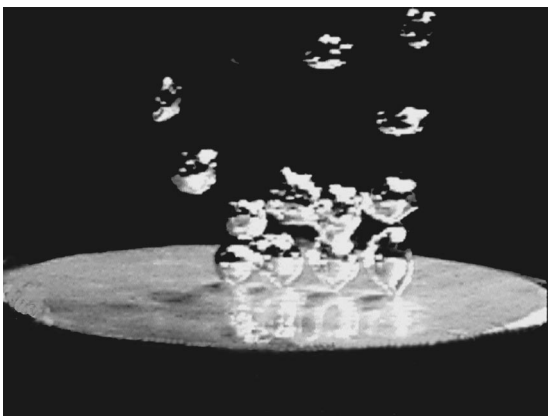

Fig. 2. Four active nucleation sites, arranged in a line.

3. Results

3.1. Isolated active nucleation site

Fig. 3 shows the relationship between the bubble diameter D_B and the heat flux q_H on a titanium and copper surface using three different diameters of the heated spot D_H. Bubble diameters are similar to those occurring in conventional, electricity-heated surfaces [14]. The first points in data series in Fig. 3 show diameters of bubbles soon after the onset of nucleation. In the observed range 1.66 mm < D_H < 5.23 mm, nucleation usually began with large bubbles whose diameter D_B decreased as q_H increased. By decreasing the heated spot diameter D_H and by increasing the effusivity of the foil, the onset of nucleation moves towards higher heat fluxes q_H.

At small heated spots, bubble diameter D_B depends on D_H, which is shown in Fig. 4. In the observed region of D_H, D_B also increases when D_H is increased, but the D_B/D_H ratio decreases. At the same D_H, the average bubble diameters were similar on both Ti and Cu foils. When the D_H was sufficiently large, in range between 6 and 8 mm, the bubble diameter D_B was no longer dependent on D_H and also at low heat fluxes

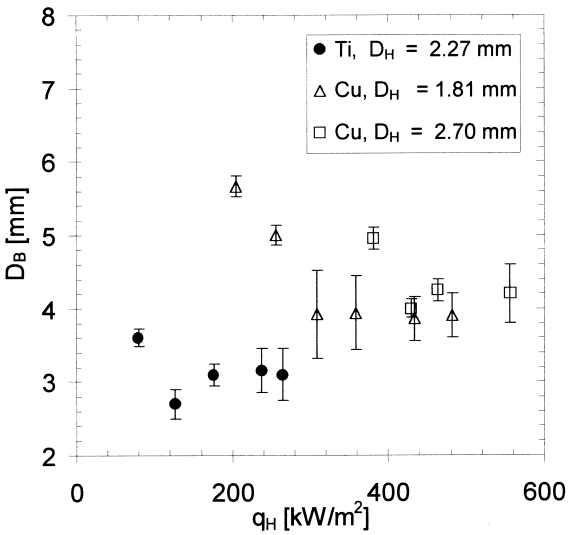

Fig. 3. Bubble diameter D_B in relation to heat flux q_H on Ti and Cu surfaces at various diameters of heated spot D_H.

more simultaneously active nucleation sites appeared on the laser heated surface.

The impact of surroundings of the nucleation site on its activity was observed by heating the surrounding surface of diameter $D_{H,\infty}$. To achieve this, first the $q_{H,\infty}$ was set just below the onset of nucleation, and then a heated spot with a diameter D_H and heat flux q_H was added within the surrounding surface of diameter $D_{H,\infty}$. In this case D_Bs were larger on both Ti and Cu foil, which is the result of more favourable conditions on the surface in the vicinity of the nucleation site. Given the same D_H, the average bubble diameters were similar on both Ti and Cu foils in the range of 25 kW/m^2 $< q_{H,\infty} <$ 30 kW/m^2. By increasing D_H, the difference between D_B with heated surrounding surface and the D_B with unheated surrounding surface decreased. In the case of large D_H, the heating of the surrounding surface no longer had an impact on D_B, because heated spot became larger than corresponding area belonging to the observed active nucleation site.

The dependence of the D_B/D_H ratio on D_H can be determined with Eqs. (3) and (4), which are given for the range 1.66 mm $< D_H <$ 5.23 mm with the heat flux in the range of 120 kW/m^2 $< q_H <$ 280 kW/m^2 for Ti foil; and 240 kW/m^2 $< q_H <$ 520 kW/m^2 for Cu foil, both foils of thickness 25 μm.

The relation between the D_B/D_H ratio and the D_H with unheated surrounding surface, $q_{H,\infty} = 0$ kW/m^2, is

$$\frac{D_B}{D_H} = 0.0424 D_H^{-0.6113}, \tag{3}$$

with the correlation coefficient 0.967, and with heated surrounding surface, $q_{H,\infty} \approx 30$ kW/m^2, it is

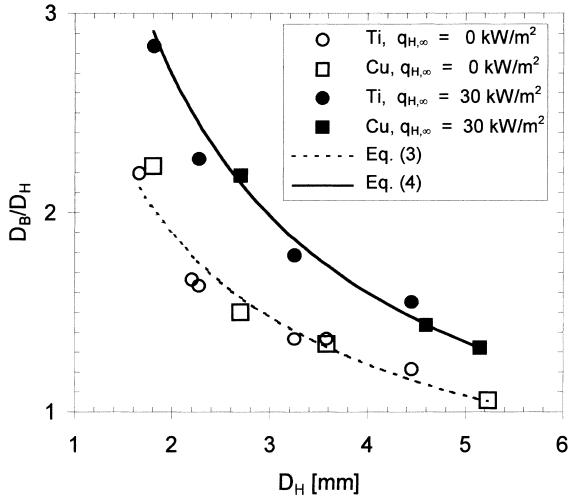

Fig. 4. Relation between the D_B/D_H ratio and the diameter of heated spot D_H.

$$\frac{D_B}{D_H} = 0.0253 D_H^{-0.7509}, \tag{4}$$

with the correlation coefficient 0.982.

3.2. Two spatially controlled active nucleation sites

In experiments involving two active nucleation sites, the configuration shown in Fig. 1(a) was used. Two heated spots of equal diameter D_H and equal heat flux q_H were placed on the arbitrary position on the surface. The surrounding surface was either heated, $q_{H,\infty} > 0$ kW/m^2, or unheated, $q_{H,\infty} = 0$ kW/m^2. The nucleation site on the left was stationary, while the right one moved across the foil. In this manner the activity, and thereby the interaction between the left and the right active nucleation site, could be observed at various distances between them. As the measure of activity of the nucleation site the released latent heat flow rate $\dot{Q}_L$ was used, which depends on bubble diameter D_B and frequency f

$$\dot{Q}_L = \frac{\pi D_B^3}{6} f \rho_v h_{fg}. \tag{5}$$

If the departing bubbles were not spherical, but had a shape of prolate ellipsoids, which were seen as ellipses in 2D pictures available, both axes of the ellipse were measured and symmetry around the third axis was presumed. With these data the equivalent diameter of sphere was calculated, which is needed for Eq. (5).

When the heated spot was moved across the test section, the activity of the nucleation sites on the heated spot, and thereby also $\dot{Q}_L$, was not constant. It was anticipated, that the scatter of the $\dot{Q}_L$ was mainly the consequence of the local surface characteristics. Larger differences between $\dot{Q}_L$s at various locations on the surface appeared at the heating of the surrounding surface. The test section was limited by the size of the foil D_F and the size of the heated surrounding heated surface $D_{H,\infty}$. Thus the measure of activity of the nucleation site was influenced also by the proximity of the edge of the heated surrounding surface and the proximity of the foil edge and was therefore corrected with the equation

$$\dot{Q}_{LC,i} = \frac{\dot{Q}_{L,i}}{K_{LC,i}}, \tag{6}$$

where $K_{LC,i}$ is the correction parameter,

$$K_{LC,i} = f\left(M, N_i, c_M, c_N, \delta(\rho c \lambda)^{0.5}\right). \tag{7}$$

$(\rho c \lambda)^{0.5}$ is effusivity of the foil with the thickness δ. M and N_i were defined as a non-dimensional distances. M is the distance of the centre of the heated surrounding surface from the foil centre, divided by $D_F/2$. N_i is the

distance of the centre of the heated spot i from the centre of the heated surrounding surface, divided by $D_{H,\infty}/2$. N_i can be expressed in relation to M

$$N_i = \frac{2}{D_{H,\infty}}\left(\left[M\frac{D_F}{2}\right]^2 - i_x[2m_x - i_x] - i_y[2m_y - i_y]\right)^{0.5}. \quad (8)$$

m_x and m_y are the co-ordinates of the centre of the heated surrounding surface; i_x and i_y are the co-ordinates of the centre of the heated spot i. The distance between the active nucleation sites i and j can be written as

$$S_{ij} = \left(\left(\frac{D_{H,\infty}}{2}\right)^2\left(N_i^2 + N_j^2\right) - \frac{1}{2}(MD_F)^2 + 2m_x(i_x + j_x) + 2m_y(i_y + j_y) - 2i_xj_x - 2i_yj_y\right)^{0.5}, \quad (9)$$

and the correction parameter $K_{LC,i}$ for nucleation site i as

$$K_{LC,i} = 1 - \left(\frac{1}{2}[D_{H,\infty} + D_H]e^{0.1\delta(\rho c\lambda)^{0.5}}\right)^{-2} \times \left(\frac{1}{4}[M^{c_M}D_F]^2 - i_x[2m_x - i_x] - i_y[2m_y - i_y]\right)^{0.5c_N}. \quad (10)$$

$K_{LC,i}$ equals unity, if the nucleation site i is in the centre of the heated surrounding surface, which is in the foil centre. The interrelated impact of the M and N_i is weighted with constants c_M and c_N, which were derived with the regression analysis of the $\dot{Q}_{L,i}$ of the single, alone functioning nucleation site i at various locations on the foil surface

$$c_M = 110D_H - 0.104\delta(\rho c\lambda)^{0.5} + 0.746, \quad (11)$$

$$c_N = 1030D_H + 0.82\delta(\rho c\lambda)^{0.5} - 1.33. \quad (12)$$

Fig. 5(a) shows $\dot{Q}_{L,C}$ and $\dot{Q}_L$ as the measure of activity for single, alone functioning active nucleation site on Ti and Cu foils on a heated and unheated surrounding surface at various D_H. Abscissa value "Position" represents the distance between the coordinates of the left (L) nucleation site and the active (A), alone functioning nucleation site. For given D_H, positions of the single active nucleation site in Fig. 5(a) are the same as positions of the right nucleation site in experiments with two active nucleation sites, shown in Fig. 5(b)–(f). Fig. 5(b) and (c) shows the activity of two nucleation sites at various distances S between them on the heated surrounding surface, $q_{H,\infty} > 0$ kW/m^2. The activity of the stationary, left (L) nucleation site, $\dot{Q}_{L,C}$ (L), the activity of the mobile, right (R) nucleation site, $\dot{Q}_{L,C}$ (R), and the sum of activities of both nucleation sites, $\dot{Q}_{L,C}$ (L) $+\dot{Q}_{L,C}$ (R) at various S are given. Fig. 5(d)–(e) shows the same situation on an unheated surrounding surface, $q_{H,\infty} = 0$ kW/m^2.

When the distance S between the nucleation sites is considerable, there is no interaction between them. In the observed region, as the two sites approach each other, interaction occurs in the form of

1. Decreased activity of both nucleation sites, or as
2. Decreased activity of one of the nucleation sites while the activity of the other nucleation site simultaneously increases.
3. Irrespective of case (i) or (ii), the consequence of the interaction between both nucleation sites is the decrease of the net released latent heat flow rate $\dot{Q}_{L,C}$ (L) $+\dot{Q}_{L,C}$ (R) or $\dot{Q}_L$ (L) $+$ $\dot{Q}_L$ (R).

Experiments with laser activated nucleation sites indicate that the nucleation sites can even help each other, but when the distances between them are sufficiently small the interaction has an adverse effect on the net activity of nucleation sites involved. In most cases the interaction became significant when the non-dimensional distance between the nucleation sites decreased to $S/D_B \approx 1$ or less on the unheated surrounding surface, $q_{H,\infty} = 0$ kW/m^2, and already at greater S/D_B on the heated surrounding surface, $q_{H,\infty} > 0$ kW/m^2.

Chekanov [10] established that a favourable exchange of influence among the nucleation sites occurs at $S/D_B > 3$, while Judd with his co-workers [11–13,18,19] determined that the nucleation sites promote each other at $S/D_B < 1$. Our results as well show that the consequence of interaction may be the improved activity of one of the nucleation sites, but only with the simultaneous deterioration of the activity of the other nucleation site in a pair, and deterioration of the collective activity, as the consequence of the net exchange of influence between the adjacent nucleation sites.

The dominant active nucleation site on the entirely heated surface occurs at the most suitable potential nucleation site, whose location is determined by the microstructure and surface topography. The occurrence of adjacent nucleation sites depends on the conditions around the dominant active nucleation site. Developed experimental technique enables activation of potential nucleation sites at an arbitrarily selected spot on the surface. The "natural occurrence" of the boiling process is thus sacrificed to some extent, but the possibility for direct measurement of the interaction is obtained.

If two nucleation sites are sufficiently close together, one of the nucleation sites may cause the other nucleation site to completely stop with activity. In this case as well the activity of the active nucleation site is smaller than the sum of activity of both alone functioning nucleation sites. For the case of two nucleation sites on Cu foil, formed on equal heated spots of diameter $D_H = 1.8$ mm with the same heat flux, $q_H = 495$ kW/m^2, the range of distance between two nucleation sites S, in which deactivation of the adjacent nucleation site occurs, is between 0.7 and 1.8 mm for the unheated surrounding surface, $q_{H,\infty} = 0$ kW/m^2. For

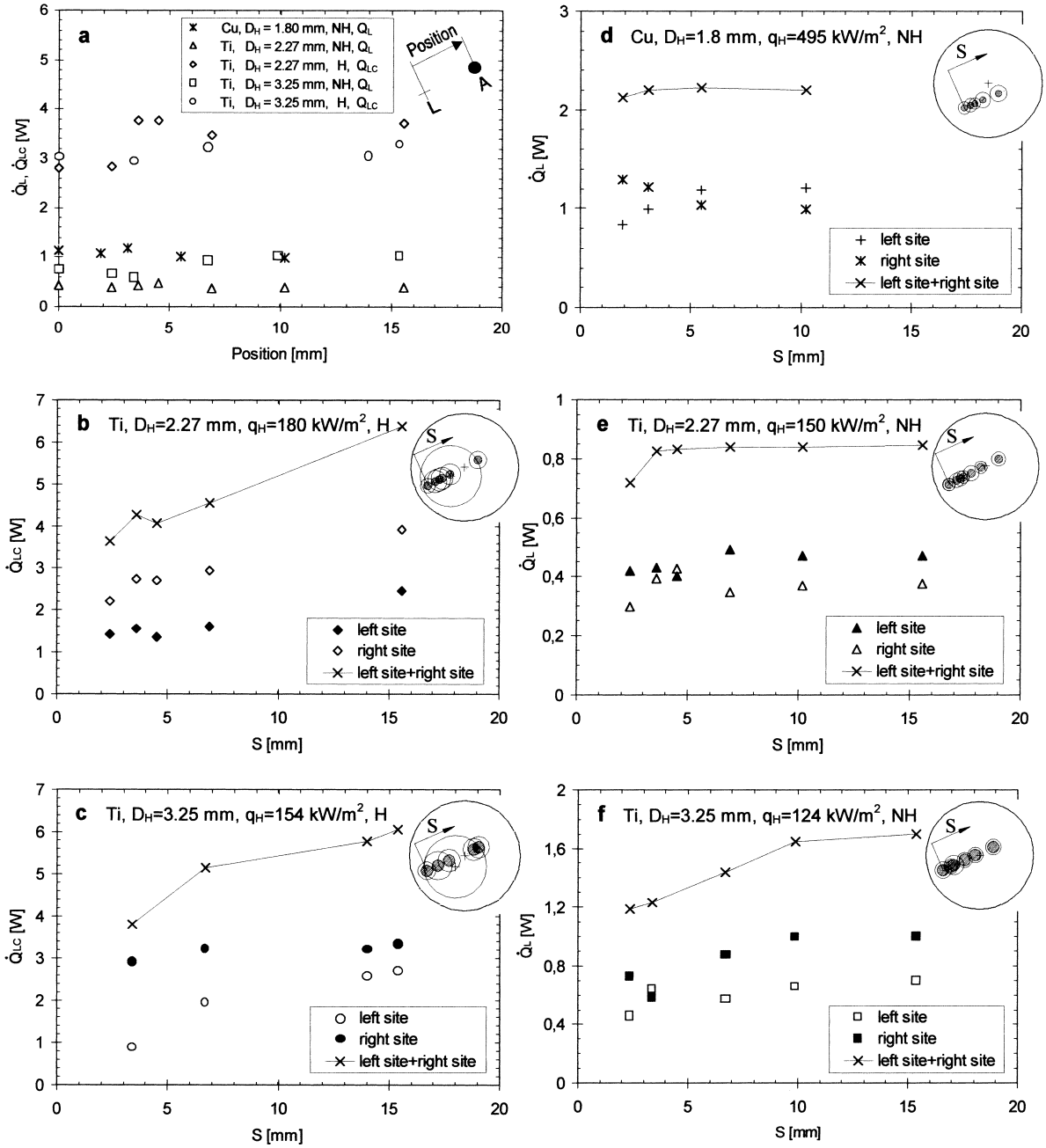

Fig. 5. $\dot{Q}_{L,C}$ and $\dot{Q}_L$ as a measure of activity for single nucleation sites at various positions, (a) and at various distances between two nucleation sites S, (b)–(e). L — coordinates of the left nucleation site; A — position of the single active nucleation site. H — surrounding surface is heated; NH — surrounding surface is not heated.

the heated surrounding surface, $q_{H,\infty} = 30$ kW/m^2, this range is shifted to larger values of S between 1.1 and 2.8 mm. Average bubble diameter of both nucleation sites, measured at the upper border of the deactivation range, were 3.5 and 4.9 mm for the heated and unheated surrounding surface, respectively.

3.3. Three or four active nucleation sites

The configuration in Fig. 1(b) was used in experiments with up to four heated spots. Each heated spot could be placed at an arbitrary selected location on the test section. The heat flux of all four heated spots, which had the same diameter D_H, could be varied. The measure of activity of the nucleation site $\dot{Q}_L$ was not corrected with Eq (6) because the surrounding surface was not heated and because all the arrangements were placed around the centre of the foil. The first arrangement was in-line, involving three or four heated spots of diameter D_H = 3.58 mm. The heated spots 1 and 2 had the same, constant heat flux, while the heat flux at heated spots 3 or/and 4 was increased. Distances between the individual heated spots S are shown on the figures.

Fig. 6(a) shows the frequency of bubble emission, and Fig. 6(b) shows the released latent heat flow rate when heat flux was increased at heated spot 3, which was located on the right hand side adjacent to heated spot 1. Spot 4 was not heated. The interaction of the nucleation sites is manifested primarily in the changes of bubble emission frequency. By increasing the heat flux at the adjacent heated spot 3, the activity of the observed nucleation site on the heated spot 1 decreased until it completely stopped. Nucleation sites on the heated spots 2 and 3 were sufficiently apart to prevent any observable interaction, not even through the nucleation site on the heated spot 1 which was placed between them.

The influence of the increased heat flux at heated spot 4, located between heated spots 1 and 2, is shown in Fig. 7(a) and (b). In this case spot 3 was not heated. Nucleation site on the heated spot 4 shared the influence with both adjacent nucleation sites on the heated spots 1 and 2. In order to deactivate nucleation site 1, about 50% greater heat flux at heated spot 4 was

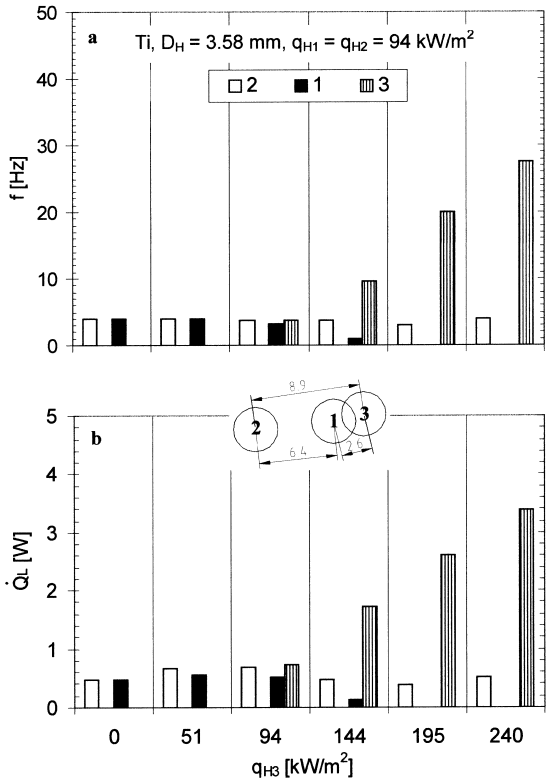

Fig. 6. Bubble frequency f and latent heat flow rate $\dot{Q}_L$ at three nucleation sites, arranged in a line. Heated spots 1 and 2 have a constant q_H, while at heated spot 3 the q_H is increased.

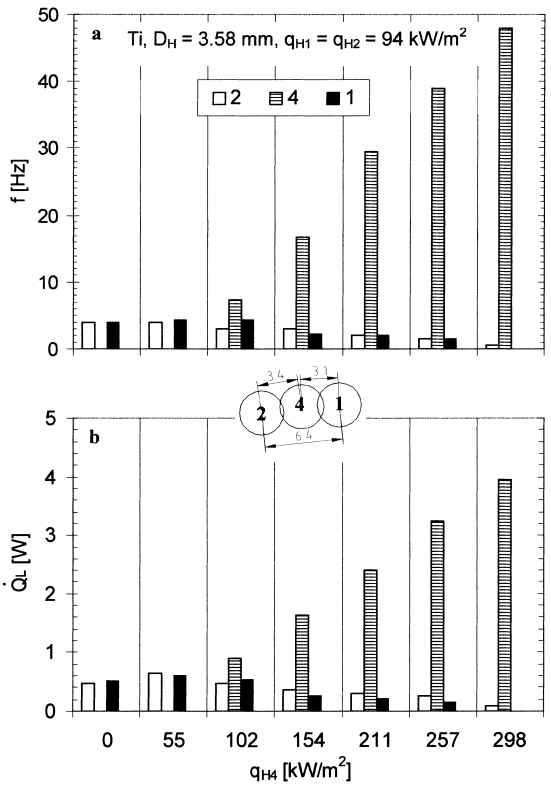

Fig. 7. Bubble frequency f and latent heat flow rate $\dot{Q}_L$ at three nucleation sites, arranged in a line. Heated spots 1 and 2 have a constant q_H, while at heated spot 4 the q_H is increased.

necessary than at heated spot 3, while the nucleation site 2 in this case as well did not completely stop functioning.

Fig. 8(a) and (b) show the activity of nucleation sites at the same arrangements, but now the heat flux at the heated spots 3 and 4 was increased at once. It is evident that the interaction takes place primarily between the adjacent nucleation sites. A much smaller heat flux at the heated spots 3 and 4 was needed for the deactivation of nucleation site 1, since the nucleation site 1 shared the influence with the two adjacent nucleation sites 3 and 4 and not only with the nucleation site 4, as in the previous example (Fig. 7) of this arrangement.

The next arrangement was two-dimensional with four heated spots of diameter $D_H = 2.2$ mm, forming a quadrangle. Fig. 9(a) shows the frequencies of bubbles at the individual nucleation sites, while Fig. 9(b) shows the corresponding latent heat flow rates. Heated spots 3 and 4 had a constant heat flux, while the heat flux was increased at heated spots 1 and 2, where $q_{H,1} = q_{H,2}$. Given a sufficiently high heat flux at heated spots 1 and 2, nucleation site 3 was deactivated, while at nucleation site 4 the activity only decreased somewhat. The difference between nucleation sites 3 and 4 was only in the location, so that the local characteristics of the surface play a significant role in the interaction between the nucleation sites. Stronger nucleation sites, occurring at more suitable surface locations, are less sensitive to the influence of adjacent nucleation sites.

With the same arrangement, the activity of nucleation sites at different number of simultaneously active nucleation sites in various combinations was observed. In this case the heat flux was the same on all four heated spots of diameter $D_H = 1.66$ mm. Fig. 10(a) shows relative changes of the frequency, f/f_0, and Fig. 10(b) relative changes of the latent heat flow rate, $\dot{Q}_L/\dot{Q}_{L,0}$, at collective activity of two, three or four nucleation sites. The f_0 and the $\dot{Q}_{L,0}$ are frequency and latent heat flow rate of the alone functioning nucleation site, respectively. At the single nucleation sites, the

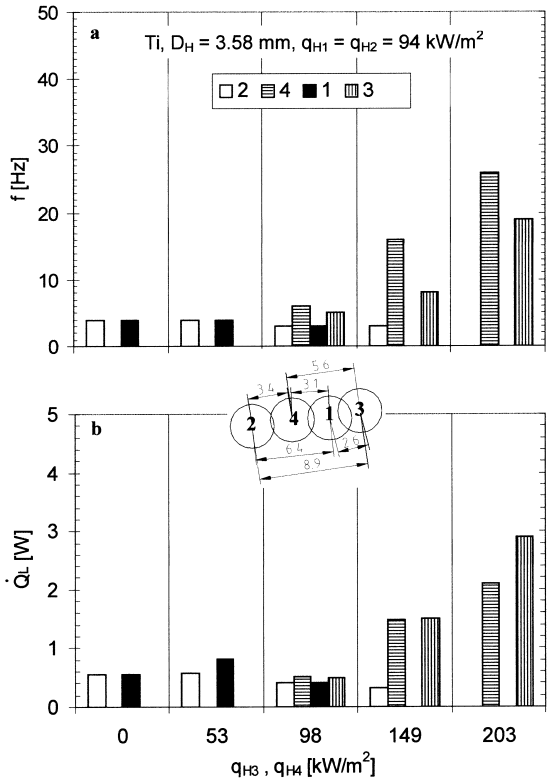

Fig. 8. Bubble frequency f and latent heat flow rate $\dot{Q}_L$ at four nucleation sites, arranged in a line. Heated spots 1 and 2 have constant q_H, while at heated spots 3 and 4 the q_H is increased.

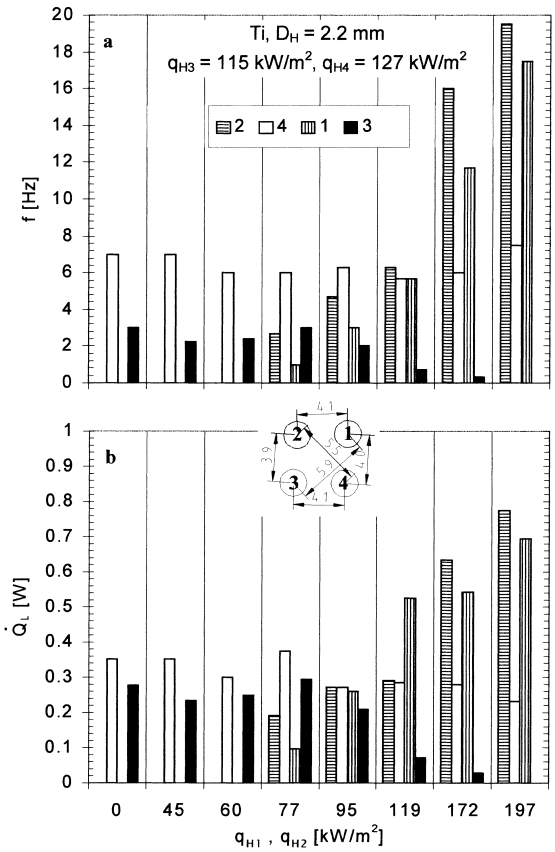

Fig. 9. Bubble frequency f and latent heat flow rate $\dot{Q}_L$ at four nucleation sites, arranged in a quadrangle. Heated spots 3 and 4 have constant q_H, while at heated spots 1 and 2 the q_H is increased.

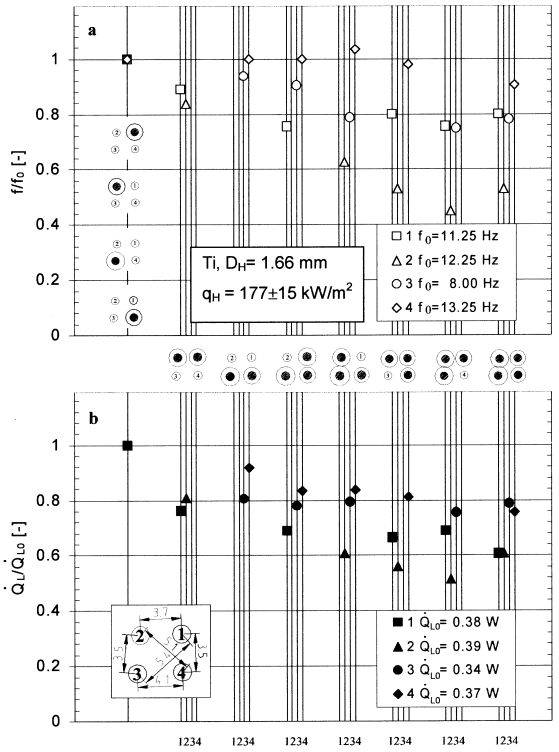

Fig. 10. Relative frequency change of bubbles f, (a) and latent heat flux $\dot{Q}_L$ (b), at four nucleation sites, arranged in a quadrangle. Individually active nucleation site has the value of f_0 and $\dot{Q}_{L,0}$. $D_H = 1.66$ mm.

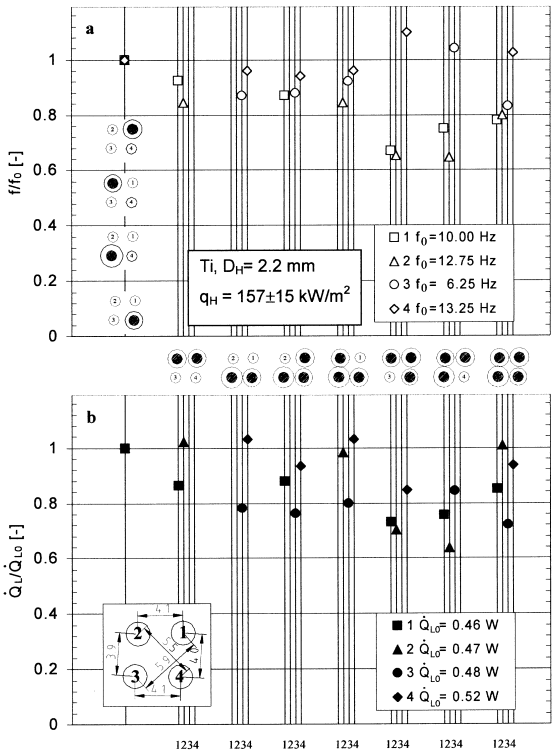

Fig. 11. Relative frequency change of bubbles f (a), and latent heat flux $\dot{Q}_L$, (b), at four nucleation sites, arranged in a quadrangle. Individually active nucleation site has the value of f_0 and $\dot{Q}_{L,0}$. $D_H = 2.2$ mm.

scatter of the frequency f_0 was within $\pm 6.7\%$. In graphic presentation of arrangements the white circles represent the unheated and the black circles the heated spots, where active nucleation sites appeared. On heated spots the average bubble diameters are shown. The group of four vertical lines represent one arrangement, and each line represents the nucleation site marked below. Fig. 11(a) and (b) are similar, showing f/f_0 and $\dot{Q}_L/\dot{Q}_{L,0}$ for $D_H = 2.2$ mm.

As can be observed, the activity of almost all nucleation sites decreases with the increase of influence of the environment, which increases with the number of surrounding active nucleation sites. The nucleation sites, formed on heated spot of smaller diameter are more sensitive to the influence of adjacent nucleation sites. The differences between f/f_0 and $\dot{Q}_L/\dot{Q}_{L,0}$ indicate that the interactions are reflected in the frequency as well as in the diameter of the bubbles. Particularly in Fig. 10(a) and (b) the influence of the local surface characteristics on the interaction between nucleation sites can be observed. The location of nucleation site 2 is evidently less favourable, and is therefore the most susceptible to the influence of adjacent nucleation sites, while nucleation site 4 is less sensitive.

4. Conclusions

The developed technique of activating nucleation sites with laser-assisted heating enables direct measuring of interactions between active nucleation sites.

The interaction between two artificially activated nucleation sites occurs as a net decrease of activity of both sites, whereby the activity of both nucleation sites may be decreased or the activity of one increases while the activity of the other simultaneously decreases. In an extreme case, one nucleation site may cause the other site to completely stop functioning. If the nucleation site has in its vicinity several adjacent nucleation sites, it shares its influence with all of them.

The developed technique of activating nucleation sites by activating or enhancing existing nucleation sites at high heat flux boiling could be used for the study of the phenomenon of interaction in the real environment.

References

[1] J.H. Lienhard, Snares of pool boiling research: putting

our history to use, in: Proceedings of 10th International Heat Transfer Conference, vol. 1, IChemE, Rugby, 1994, pp. 333–348.
[2] A.E. Bergles, What is the real mechanism of CHF in pool boiling, in: Proceedings of Engineering Foundation Conference on Pool and External Flow Boiling, ASME, New York, 1992, pp. 165–170.
[3] P. Sadasivan, C. Unal, R.A. Nelson, Nonlinear aspects of high heat flux nucleate boiling heat transfer, ASME Journal of Heat Transfer 117 (1995) 981–989.
[4] I. Golobič, E. Pavlovič, S. Strgar, D.B.R. Kenning, Y. Yan, Wall temperature variations during bubble growth on a thin plate: computations and experiments, in: Eurotherm Seminar No. 48: Pool Boiling 2, ETS, Pisa, 1996, pp. 25–32.
[5] D. Gorenflo, A. Luke, E. Danger, Interactions between heat transfer and bubble formation in nucleate boiling, in: Proceedings of the Eleventh International Heat Transfer Conference, vol. 1, Kyongju, 1998, pp. 149–174.
[6] R.A. Nelson, D.B.R. Kenning, M. Shoji, Nonlinear dynamics in boiling phenomena, Journal of Heat Transfer Society of Japan 35 (1996) 22–34.
[7] M. Shoji, Boiling chaos and modeling, in: Proceedings of the Eleventh International Heat Transfer Conference, vol. 1, Kyongju, 1998, pp. 3–21.
[8] H. Gjerkeš, I. Golobič, B. Gašperšič, Experimental study of interactions between spatially controlled nucleation sites on a thin flat plate in pool boiling, in: Proceedings of the International Engineering Foundation 3rd Conference: Convective Flow and Pool Boiling, Taylor & Francis, Philadelphia, 1999, pp. 111–117.
[9] H. Gjerkeš, I. Golobič, Pool boiling CHF on laser heated thin plate. International Journal of Heat and Mass transfer 43 (2000) 1999–2008.
[10] V.V. Chekanov, Interaction of centers in nucleate boiling, Teplofizika Vysokih Temperatur 15 (1977) 121–128.
[11] R.L. Judd, K.S. Hwang, A comprehensive model for nucleate pool boiling heat transfer including microlayer evaporation, ASME Journal of Heat Transfer 98 (1976) 623–629.
[12] R.L. Judd, C.H. Lavdas, The nature of nucleation sites interaction, ASME Journal of Heat Transfer 102 (1980) 461–464.
[13] R.L. Judd, A. Chopra, Interactions of the nucleation processes occurring at adjacent nucleation sites, ASME Journal of Heat Transfer 115 (1993) 955–962.
[14] R.F. Gaertner, Photographic study of nucleate pool boiling on a horizontal surface, ASME Journal of Heat Transfer 85 (1965) 17–29.
[15] R.L. Judd, On nucleation site interaction, ASME Journal of Heat Transfer 110 (1988) 475–478.
[16] C.H. Wang, V.K. Dhir, Effect of surface wettability on active nucleation site density during pool boiling of water on a vertical surface, ASME Journal of Heat Transfer 115 (1993) 659–669.
[17] R.J. Benjamin, A.R. Balakrishnan, Nucleate pool boiling heat transfer at low to moderate heat fluxes, International Journal of Heat and Mass Transfer 39 (1996) 2495–2504.
[18] M. Sultan, R.L. Judd, Spatial distribution of active sites and bubble flux density, ASME Journal of Heat Transfer 100 (1978) 56–62.
[19] A. Calka, R.L. Judd, Some aspects of the interactions among nucleation sites during saturated nucleate boiling, International Journal of Heat and Mass Transfer 28 (1985) 2331–2342.